Journal of ELECTRICAL ENGINEERING, VOL. 58, NO. 7/s, 2007, 86–92

ESTIMATE OF THE CELL NUMBER GROWTH RATE USING PDE METHODS OF IMAGE PROCESSING AND TIME SERIES ANALYSIS

Oľga Drblíková et al *

We introduce a method of how to estimate mathematically and computationally and how to analyse statistically the growth rate of the number of cells in development of the zebrafish embryo. Our method is based on analysis of 3D confocal image sequences and consists of four basic steps. First, we filter images by the geodesic mean curvature flow (GMCF) method. Then we use the flux-based level set center detection (FBLSCD) to find the approximate positions and number of the nuclei centers. In the third step we correct FBLSCD result by image segmentation algorithm based on the subjective surface (SUBSURF) method. Finally, we understand the nuclei numbers extracted by the image processing algorithmic chain as a measurements and apply the statistical methods of the time series analysis to estimate trend of the cell number growth rate. We apply the developed method to the sequences of real 3D images acquised in vivo at early stages of zebrafish embryogenesis.

K e y w o r d s: nonlinear advection-diffusion equations, numerical solution, flux-based level set method, subjective surface method, image processing, embryogenesis

2000 *Mathematics Subject Classification*: 35K55, 74S10, 92C55, 92C37

1 INTRODUCTION

In this paper we develop a strategy of extracting the cell number growth rate from the 3D image sequences representing acquisition of the first hours of zebrafish embryogenesis.

Since a noise is intrinsically linked to the image acquisition, as the first step, we use nonlinear diffusion method to filter the images. We provide this operation by a few steps of the so-called geodesic mean curvature flow (GMCF) model in its semi-implicit finite volume implementation [5]. Then we apply the flux-based level set center detection (FBLSCD) method [3] to extract the approximate positions of centers, and consequently the approximate number, of nuclei. FBLSCD is an evolutionary numerical method based on flux-based finite volume discretization [2] of an advection-diffusion formulation of the morphological operators which is followed by a detection of the local maxima of the evolving function. The process is stopped when the rate of decrease of the number of local maxima is bellow some chosen threshold. In order to prevent false negative events (i.e. that nucleus is there but its center is not detected) we choose higher threshold and consequently we can slightly over-estimate the true nuclei number, e.g. we can detect more centers (false positive event) in one nucleus. In the third step, we correct the estimates given by the FBLSCD by the subjective surface (SUBSURF) image segmentation method [9] in its semi-implicit finite volume implementation [1, 7]. Starting from true and superfluous centers in one nucleus we end up with the same segmentation result which allow us to reduce relialably the nuclei number in every 3D image of the sequence.

The final step of our approach is an application of the time series analysis methods to the extracted number of nuclei during the embryogenesis. Understanding the image acquisition followed by the above chain of image processing algorithms as a measurement, we may use the statistical approach to find a trend of the cell number growth rate.

In the next section we discuss the mathematical models and computational algorithms used in our image processing approach. In the last section we present and discuss statistical time series analysis results.

2 IMAGE ANALYSIS ALGORITHMS BASED ON PDEs AND THEIR DISCRETIZATION

Any 3D nuclei image in the zebrafish embryogenesis time sequence is given by a scalar (greylevel) intensity function $u_N^0 \colon \Omega \to R$, $\Omega \subset R^3$. Without loss of generality we may assume that $0 \leq u_n^0 \leq 1$.

Nowadays, it is possible to label the zebrafish embryo cells and to obtain well contrasted laser scanning microscopy 3D images throughout embryonic development

* O. Drblíková, M. Komorníková, K. Mikula, M. Remešíková, Department of Mathematics, Slovak University of Technology, Faculty of Civil Engineering, Radlinského 11, 813 68 Bratislava. E-mail: {drblikov,magda,mikula,remesik}@math.sk,

P. Bourgine, CREA - Ecole Polytechnique, Paris, France. E-mail: bourgine@shs.polytechnique.fr

N. Peyriéras, CNRS-DEPSN, Institut de Neurobiologie Alfred Fessard, Batiment 32-33, Avenue de la Terrasse, 91198 Gif sur Yvette, France. E-mail: nadine.peyrieras@iaf.cnrs-gif.fr

A. Sarti, DEIS, University of Bologna, Bologna, Italy. E-mail: asarti@deis.unibo.it

ISSN 1335-3632

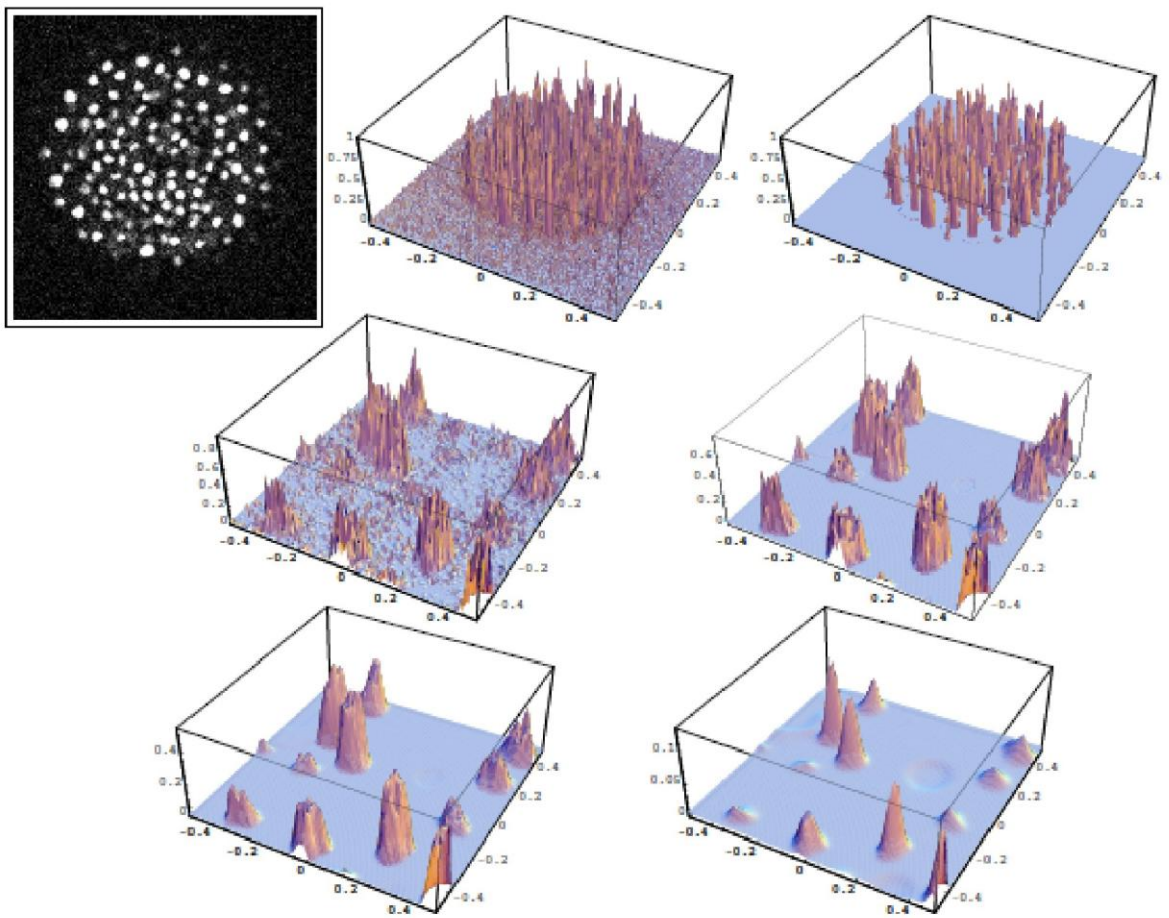

Fig. 1. Top row: 2D slice of 3D volume (left), its noisy greylevel intensity as a graph (middle) and filtered intensity by GMCF (right). Next four images show details of image intensity before filtering (middle-left), after filtering (middle-right), and solution u of FBLSCD after 5 (left-bottom) and 26 time steps (right-bottom) when the process is stopped and local maxima give the nuclei centers.

of alive animal. However, a noise is intrinsically linked to the scanning technique and any image analysis algorithms have to deal with it. First, the image processing methods devoted, e.g., to counting the number of cells and extraction of the approximate cell centers [3], the methods for the cell segmentation [10,3], the cell tracking and the velocity field extraction [6] need to reduce spurious, noisy structures, they simply cannot work with highly noisy images. The second reason is that all the mentioned methods are computationally much faster when applied to properly filtered image sequences. Thus, the first step of our image processing chain is a filtering. To that goal we use the so-called geodesic mean curvature flow in the level set formulation. The model equation for the GMCF filtering reads as follows

$$u_t = |\nabla u| \nabla \cdot \left(g(|\nabla G_\sigma * u|) \frac{\nabla u}{|\nabla u|} \right) \qquad (1)$$

starting with the initial condition $u(0,x) = u_N^0(x)$ and considering the zero Neumann boundary conditions on the boundary of image domain $\partial\Omega$. In the model, the mean curvature driven motion of image level sets is influenced by the edge indicator function $g(s) = 1/(1+Ks^2)$ applied to the evolving image intensity (presmoothed by the Gaussian kernel with a small variance σ). Such diffusion term causes accumulation of level sets along the object boundaries and thus edge preserving filtering. The equation (1) is discretized by the finite volume scheme in space and semi-implicit approach in time and we used to provide few time steps to get the filtered result. We denote it by $u_{N_f}^0$ and it is equal to solution u of (1) at the filtering stopping time T_f. A careful quantitative study of the filtering properties of nonlinear diffusion models is given in [5] showing that GMCF has very good capability to remove noise and sharpen unspurious image structures.

The second step in our approach is the flux-based level set center detection. In FBLSCD we utilize a specific feature of the images where the nuclei are given by (noisy) humps of the image intensity, cf. Fig. 1. We can see that humps representing nuclei are composed by level sets with relatively large diameter r_1, $0 \ll c_1 \leq r_1 \leq c_2$, while diameter r_2 of level sets representing spurious structures

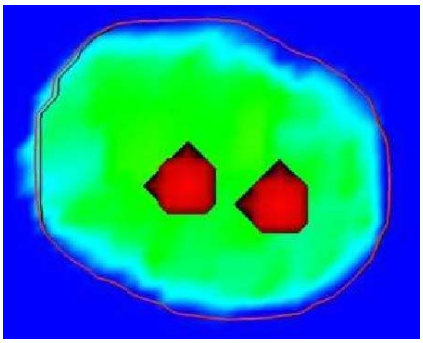

Fig. 2. Two detected centers in one nucleus together with their almost identical shapes found after segmentation.

(still due to a noise) is much smaller, close to zero, $0 < r_2 \ll c_1$. In general, the level sets are closed surfaces, and, if they are moving at a constant speed in direction of inner normal vector field the encompassing volume is decreasing and finally they disappear. The level sets with a small diameter, representing a spurious structures, disappear (shrink) in a fast way, while level sets representing real image objects remain for much longer time during such evolution (they are observable in long time-scales).

It is also well-known that if the evolution of surfaces depends on the local mean curvature then a speed of shrinking tends to infinity as diameter of level set tends to zero, cf. e.g. [4]. We use this fact to even speed up the shrinking in the above mentioned advective mechanism. Then the evolutionary process of level sets can be represented by a geometrical equation $V = \delta + \mu k$, where the normal velocity V is given by a constant δ plus the mean curvature k multiplied by a positive constant μ. The level set formulation is then given by the equation

$$\partial_t u = \delta \frac{\nabla u}{|\nabla u|} \cdot \nabla u + \mu |\nabla u| \nabla \cdot \left(\frac{\nabla u}{|\nabla u|} \right) \qquad (2)$$

applied to the initial condition $u^0_{N_f}$. Due to the shrinking and smoothing of solution to (2), we observe a decrease of number of the local maxima which is fast at the beginning of the process and which is stabilized in time. We stop the evolutionary process when a slope of decreasing is bellow a certain threshold. The positions and number of the local maxima at the stopping time T_c is the output of FBLSCD algorithm, cf Fig. 1.

In order to prevent false negative events (i.e. that nucleus is there but its center is not detected) we choose higher threshold to stop FBLSCD and consequently we slightly over-estimate the true nuclei number. E.g. we can detect more centers in one nucleus (false positive event), but, on the other side, it prevents a loss of nuclei with low intensity. In spite of choosing a lower threshold, we prefer to correct the result of the FBLSCD and remove possible superfluous centers by the subjective surface image segmentation.

In SUBSURF method we assume that $s_l, l = 1, \ldots, S$ are points in R^3 where the approximate nuclei centers were detected. To start the nucleus segmentation, first, the initial segmentation function $u^0_{s_l}$ is constructed for every $l = 1, \ldots, S$. It is given by value 1 in a small ball centered in s_l and by value 0 outside the ball. A radius of the ball depends on a distance of the other closest centers. Then, in order to extract the nucleus shape, we evolve all the initial segmentation functions by solving the subjective surface equation [9]

$$\partial_t u = \sqrt{\varepsilon^2 + |\nabla u|^2} \nabla \cdot \left(g(|\nabla G_\sigma * u^0_{N_f}|) \frac{\nabla u}{\sqrt{\varepsilon^2 + |\nabla u|^2}} \right), \quad (3)$$

with ε a parameter, accompanied by Dirichlet boundary conditions, on a subdomain of Ω sufficiently covering the potential nucleus shape. Let us note that the solutions can be done in parallel for different (families of) nuclei. By the equation (3), the solution evolves to a "piecewise constant steady state" which gives the result of the segmentation process. As the criterion to recognize the "steady state" we check whether squared L_2 norm of difference in solution between subsequent time steps is less than a threshold α. To extract the nucleus shape we take a level surface in the middle of the shock profile at the stopping time T_s. Figure 2 depicts an example when starting from two detected centers we obtain almost identical segmented shapes which allow us to remove the superfluous center. We show also Fig. 3 with zoom of 3D volume where several superfluous centers were removed by the image segmentation. Let us note that we choose this subvolume for illustration, usually the correction of FBLSCD result is needed only for about five percent of nuclei in the whole volume.

2.1 Discretization of PDE models

Let T, the stopping time of the algorithms, equal either to T_f, T_c or T_s. For every method we choose discrete time step τ, then $T = N\tau$ where N is a total number of steps of the method. The variance σ is also fixed in advance. Let us note that we realize convolution with the Gaussian by solving linear heat equation numerically for a short time corresponding to σ. We derive in a detail the scheme for GMCF method. Such scheme is then simply adjusted to SUBSURF model and, finally, adding an upwind term we end up with a discrete FBLSCD algorithm.

To get the schemes, at first we replace the time derivative in the equation (1) by the backward difference and nonlinear terms are considered at the previous time step while linear terms are taken at the current time level. In such a way we get the semi-implicit time discretization

$$\frac{1}{|\nabla u^{n-1}|} \frac{u^n - u^{n-1}}{k} - \nabla \cdot \left(g(|\nabla u^{n-1}_\sigma|) \frac{\nabla u^n}{|\nabla u^{n-1}|} \right) = 0 \quad (4)$$

where we use notation $u^{n-1}_\sigma = G_\sigma * u^{n-1}$, and u^n represents solution at the n-th filtering step, starting by $u^0 = u^0_N$.

For the spatial discretization we employ the so-called finite volume method. We identify the finite volume mesh

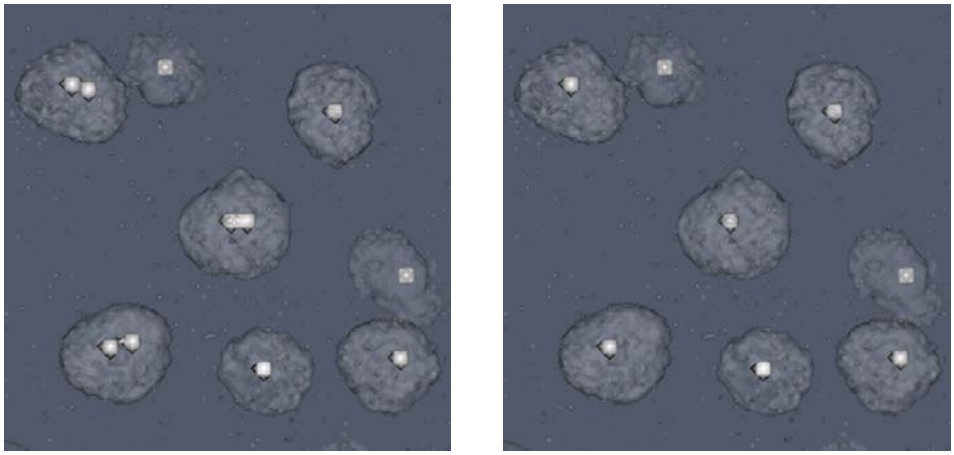

Fig. 3. Removing of superfluous nuclei centers. The centers are visualized as small balls and nuclei by isosurfaces. Left: centers detected by FBLSCD. Right: centers after SUBSURF segmentation.

$\mathcal{T}_h$ with the voxels of 3D image and denote each finite volume by V_{ijk}, $i = 1,\dots,N_1$, $j = 1,\dots,N_2$, $k = 1,\dots,N_3$. For each $V_{ijk} \in \mathcal{T}_h$ let N_{ijk} denote the neighbours index shift, i.e. the set of all (p,q,r), such that $p,q,r \in \{-1,0,1\}$, $|p|+|q|+|r| = 1$. Let $m(V_{ijk})$ denote volume of V_{ijk}. The line connecting center of V_{ijk} and center of its neighbour $V_{i+p,j+q,k+r}$, $(p,q,r) \in N_{ijk}$ is denoted by σ_{ijk}^{pqr} and its length by h_{ijk}^{pqr}. Since our finite volume grid is regular rectangular we use also shorter notations h_1 for $h_{ijk}^{p00}, p \in \{-1,1\}$, h_2 for $h_{ijk}^{0q0}, q \in \{-1,1\}$ and h_3 for h_{ijk}^{00r}, $r \in \{-1,1\}$ representing size of finite volumes in x_1, x_2, x_3 direction, respectively. The planar sides of finite volume V_{ijk} are denoted by e_{ijk}^{pqr} with area $m(e_{ijk}^{pqr})$. Let x_{ijk}^{pqr} be point where the line σ_{ijk}^{pqr} crosses the side e_{ijk}^{pqr}. We integrate (4) over every finite volume V_{ijk} and get

$$\int\limits_{V_{ijk}} \frac{1}{|\nabla u^{n-1}|}\frac{u^n - u^{n-1}}{\tau}\mathrm{d}x = \int\limits_{V_{ijk}} \nabla\cdot\Big(g(|\nabla u_\sigma^{n-1}|)\frac{\nabla u^n}{|\nabla u^{n-1}|}\Big)\mathrm{d}x\,. \quad (5)$$

Let u_{ijk}^n be fully discrete approximate solution, representing value inside the finite volume V_{ijk} at the n-th time step. We can naturally express the left hand side of (5) as

$$\int\limits_{V_{ijk}} \frac{1}{|\nabla u^{n-1}|}\frac{u^n - u^{n-1}}{\tau}\mathrm{d}x \approx \frac{m(V_{ijk})}{\overline{Q}_{ijk}^{n-1}}\,\frac{u_{ijk}^n - u_{ijk}^{n-1}}{\tau} \quad (6)$$

where $\overline{Q}_{ijk}^{n-1}$ is an average modulus of gradient in V_{ijk}, cf. [4]. For the right hand side of (5) using divergence theorem we get

$$\int\limits_{V_{ijk}} \nabla\cdot\Big(g(|\nabla u_\sigma^{n-1}|)\frac{\nabla u^n}{|\nabla u^{n-1}|}\Big)\mathrm{d}x = \sum_{|p|+|q|+|r|=1}\int\limits_{e_{ijk}^{pqr}} \frac{g(|\nabla u_\sigma^{n-1}|)}{|\nabla u^{n-1}|}\frac{\partial u^n}{\partial \nu_{ijk}^{pqr}}\mathrm{d}s\,. \quad (7)$$

Here, the derivative in direction of unit normal ν_{ijk}^{pqr} to the side e_{ijk}^{pqr} is approximated by the finite difference of neighbouring voxel values divided by the distance between voxel centers. To approximate modulus of gradients on voxel sides, we use the following definitions for $p,q,r \in \{-1,0,1\}$, $|p|+|q|+|r| = 1$,

$$\nabla^{p00}u_{ijk}^n = \Big(p\frac{u_{i+p,j,k}^n - u_{ijk}^n}{h_1}, \frac{u_{ijk}^{p10} - u_{ijk}^{p,-1,0}}{h_2}, \frac{u_{ijk}^{p01} - u_{ijk}^{p,0,-1}}{h_3}\Big), \quad (8)$$

$$\nabla^{0q0}u_{ijk}^n = \Big(\frac{u_{ijk}^{1q0} - u_{ijk}^{-1,q,0}}{h_1}, q\frac{u_{i,j+q,k}^n - u_{ijk}^n}{h_2}, \frac{u_{ijk}^{0q1} - u_{ijk}^{0,q,-1}}{h_3}\Big), \quad (9)$$

$$\nabla^{00r}u_{ijk}^n = \Big(\frac{u_{ijk}^{10r} - u_{ijk}^{-1,0,r}}{h_1}, \frac{u_{ijk}^{01r} - u_{ijk}^{0,-1,r}}{h_2}, r\frac{u_{i,j,k+r}^n - u_{ijk}^n}{h_3}\Big) \quad (10)$$

where

$$u_{ijk}^{pq0} = \frac{1}{4}(u_{ijk}^n + u_{i+p,j,k}^n + u_{i,j+q,k}^n + u_{i+p,j+q,k}^n)\,, \quad (11)$$

$$u_{ijk}^{p0r} = \frac{1}{4}(u_{ijk}^n + u_{i+p,j,k}^n + u_{i,j,k+r}^n + u_{i+p,j,k+r}^n)\,, \quad (12)$$

$$u_{ijk}^{0qr} = \frac{1}{4}(u_{ijk}^n + u_{i,j+q,k}^n + u_{i,j,k+r}^n + u_{i,j+q,k+r}^n)\,. \quad (13)$$

The formulas (8)–(10) can be understood as an approximation of the gradient in the point x_{ijk}^{pqr}, a barycenter of e_{ijk}^{pqr}. Now we define

$$Q_{ijk}^{pqr;n-1} = \sqrt{\varepsilon^2 + |\nabla^{pqr}u_{ijk}^{n-1}|^2}\,,$$

$$\overline{Q}_{ijk}^{n-1} = \sqrt{\varepsilon^2 + \frac{1}{6}\sum_{|p|+|q|+|r|=1}|\nabla^{pqr}u_{ijk}^{n-1}|^2}$$

as an ε-regularized absolute value of the gradient on voxel sides, and, the regularized averaged gradient inside

the finite volume, respectively, computed by the solution known from the previous step $n-1$. Similarly we compute the edge indicator, where the function g is applied to the gradient of convolved solution u_σ on voxel sides, namely we define

$$g_{ijk}^{pqr;n-1} = g(|\nabla^{pqr} u_{\sigma;ijk}^{n-1}|)\,.$$

Combining all the above considerations we end up with approximation of the right hand side of (7) by following term

$$\sum_{|p|+|q|+|r|=1} m(e_{ijk}^{pqr}) \frac{g_{ijk}^{pqr;n-1}}{Q_{ijk}^{pqr;n-1}} \frac{u_{i+p,j+q,k+r}^{n} - u_{ijk}^{n}}{h_{ijk}^{pqr}}\,. \quad (14)$$

If we put together (6) and (14) and consider zero Neumann boundary conditions, we can write following linear system of equations for unknows u_{ijk}^n, $i = 1,\ldots,N_1$, $j = 1,\ldots,N_2$, $k = 1,\ldots,N_3$, which has to be solved at every discrete step n in order to provide one step of **GMCF filtering**:

$$\sum_{|p|+|q|+|r|\le 1} A_{ijk}^{pqr}\;\; u_{i+p,j+q,k+r}^{n} = u_{ijk}^{n-1}\,, \quad (15)$$

with coefficients defined as follows

$$A_{ijk}^{pqr} = -\frac{\tau\; m(e_{ijk}^{pqr}) g_{ijk}^{pqr;n-1} \overline{Q}_{ijk}^{n-1}}{m(V_{ijk}) Q_{ijk}^{pqr;n-1} h_{ijk}^{pqr}}\,, \; |p|+|q|+|r| = 1\,, \quad x_{ijk}^{pqr} \notin \partial\Omega \quad (16)$$

$$A_{ijk}^{000} = 1 + \sum_{|p|+|q|+|r|=1} -A_{ijk}^{pqr}\,, \qquad A_{ijk}^{pqr} = 0\,, \;\; \text{otherwise.}$$

Similarly, one step of **SUBSURF segmentation** is given by (15) and coefficients (16) with the only differences given by the facts that we have to incorporate (in a standard way) the zero Dirichlet boundary conditions and that the term $g_{ijk}^{pqr;n-1}$ is not updated at every step but is computed only at the beginning so it is replaced by $g_{ijk}^{pqr;0} = g\big(|\nabla^{pqr} u_{N_f,\sigma;ijk}^{0}|\big)$.

To introduce the finite volume discretization of (2), we define the velocity field $v = -\delta \frac{\nabla u}{|\nabla u|}$, and consider advective part of (2), $\partial_t u + v \cdot \nabla u = 0$, in the equivalent divergent form $\partial_t u + \nabla \cdot (v\,u) - u \nabla \cdot v = 0$. Then we integrate it in every finite volume V_{ijk} and approximate the integrated fluxes $\int\limits_{e_{ijk}^{pqr}} v(\gamma) \cdot \nu_{ijk}^{pqr} \mathrm{d}\gamma$ on boundaries of finite volume by

$$v_{ijk}^{pqr} = -\delta\; m(e_{ijk}^{pqr}) \frac{\nabla^{pqr} u_{ijk}^{n-1}}{Q_{ijk}^{pqr;n-1}} \cdot \nu_{ijk}^{pqr} \quad (17)$$

and distinguish between the outflow and inflow boundaries by defining two sets of indices $N_{ijk}^{out} = \{(p,q,r) \in N_{ijk}\,,\; v_{ijk}^{pqr} > 0\}$, $N_{ijk}^{in} := \{(p,q,r) \in N_{ijk}\,,\; v_{ijk}^{pqr} \le 0\}$. Considering a piecewise constant approximation of u in finite volumes and discrete time intervals, applying the upwind principle and Green's formula we get the following finite volume scheme for the advective part

$$m(V_{ijk}) u_{ijk}^{n} = m(V_{ijk}) u_{ijk}^{n-1} - \tau \sum_{(p,q,r)\in N_{ijk}^{out}} u_{ijk}^{n-1}\, v_{ijk}^{pqr} -$$

$$\tau \sum_{(p,q,r)\in N_{ijk}^{in}} u_{i+p,j+q,k+r}^{n-1}\, v_{ijk}^{pqr} + \tau\, u_{ijk}^{n-1} \tau \sum_{(p,q,r)\in N_{ijk}} v_{ijk}^{pqr}\,, \quad (18)$$

which can be further simplified to

$$u_{ijk}^{n} = u_{ijk}^{n-1}\Big(1 - \frac{\tau\; v_{ijk}^{in}}{m(V_{ijk})}\Big) - \frac{\tau}{m(V_{ijk})} \sum_{(p,q,r)\in N_{ijk}^{in}} u_{i+p,j+q,k+r}^{n-1}\, v_{ijk}^{pqr}\,, \quad (19)$$

with $v_{ijk}^{in} = -\sum\limits_{(p,q,r)\in N_{ijk}^{in}} v_{ijk}^{pqr}$ denoting the total inflow flux. If we put together discretization of the mean curvature flow part (i.e. the system (15) with $g \equiv 1$), the above upwind scheme for advective part and the zero Neumann boundary conditions, we end up with the following system, with just slightly more complicated right hand side as in (15), which is solved as one discrete step of **FBLSCD method**:

$$\sum_{|p|+|q|+|r|\le 1} A_{ijk}^{pqr}\;\; u_{i+p,j+q,k+r}^{n} = u_{ijk}^{n-1}\Big(1 - \frac{\tau\; v_{ijk}^{in}}{m(V_{ijk})}\Big) - \frac{\tau}{m(V_{ijk})} \sum_{(p,q,r)\in N_{ijk}^{in}} u_{i+p,j+q,k+r}^{n-1}\, v_{ijk}^{pqr}\,, \quad (20)$$

with matrix coefficients defined as follows

$$A_{ijk}^{pqr} = -\mu \frac{\tau\; m(e_{ijk}^{pqr})\, \overline{Q}_{ijk}^{n-1}}{m(V_{ijk})\, Q_{ijk}^{pqr;n-1}\, h_{ijk}^{pqr}}\,, \quad |p|+|q|+|r| = 1\,, \quad x_{ijk}^{pqr} \notin \partial\Omega \quad (21)$$

$$A_{ijk}^{000} = 1 + \sum_{|p|+|q|+|r|=1} -A_{ijk}^{pqr}\,, \quad A_{ijk}^{pqr} = 0\,, \; \text{otherwise.}$$

Since the structure of linear system for all the methods is the same and suitable for using iterative solvers, we use the so-called successive over relaxation (SOR) method, which is a modification of the Gauss-Seidel method to speed up its convergence.

In all the discretizations we use spatial dimension of the voxel equals to 0.01, then discrete time step τ for filtering is 0.001 and $K = 5$, for the segmentation τ can be larger, we use e.g. 0.01 and we use also much higher $K = 100$. In both cases convolution time step sigma is equal 0.0001. For FBLSCD we have to fulfil CFL condition, so we use time step $\tau = 0.00125$, since we usually consider small ammout of mean curvature driven diffusion, $\mu = 0.001$, and unit advection with $\delta = 1$.

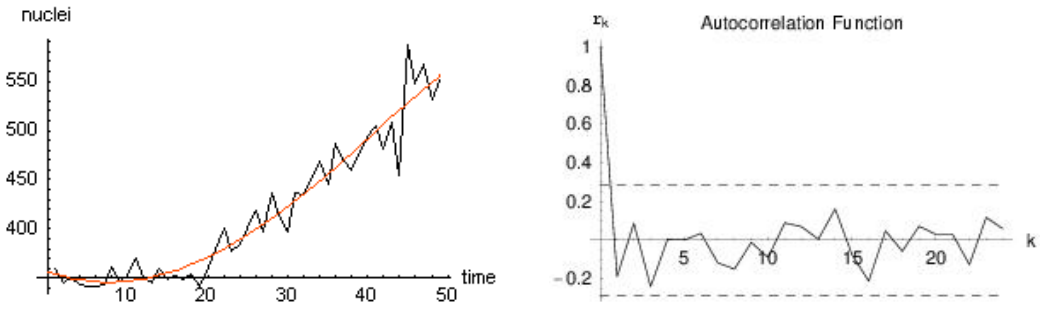

Fig. 4. Left: Plot of the first time series and the trend function. Right: Plot of the autocorrelation function.

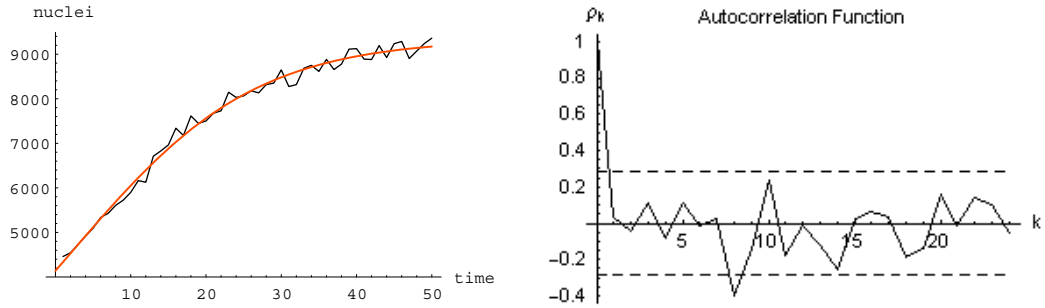

Fig. 5. Left: Plot of the second time series and the trend function. Right: Plot of the autocorrelation function.

3 TIME SERIES ANALYSIS

In this section we analyse time series z_j, $j = 1, \ldots, M$, of the nuclei numbers obtained by the PDE image processing methods. We use two data sets from which we have extracted the nuclei numbers. The first one represents 3D + time aqusition of only partially covered embryo, i.e. the cells are dividing but they also migrate in and out of volume. In this data set, there are several hundreds of cells observed in the volume during the covered time period represented by 50 time points, cf. Fig. 1 for illustration of image quality. In the second set of analysed data , there are several thousands of cells, volume of acqusition covers all the embryo and we have again 50 time points.

In our time series analysis, we try to fit the data by models of polynomial, exponential and logistic type (as well as by their combinations) which is reasonable choice for modelling the cell development. The best fit of a trend function is determined by the lowest value of the sum of squared residuals as well as by the lowest absolute values of the autocorrelation function. The goal is to find a trend function which fits data in a best way and for which residuals are uncorrelated, i.e. for all lags $k > 0$ the estimate

$$r_k = \sum_{j=1}^{M-k} (z_j - \overline{z})(z_{j+k} - \overline{z}) \Big/ \sum_{j=1}^{M} (z_j - \overline{z})^2$$

of the autocorrelation function fulfils the criterion $|r_k| < 2/\sqrt{M}$.

For the first time series the best fit of trend was obtained in the class of functions $y_t = \alpha\left(1 + \beta e^{\gamma t} + \delta t^2\right)$ with the particular form after estimation of coefficients

$$y_t = 432.064\left(1 - 0.175156e^{0.0371087t} + 0.000568795t^2\right). \tag{22}$$

As we can see in Fig. 4 left, the trend function is slightly decreasing in the right neighbourhood of the origin and, after attaining a single minimum, it subsequently increase and well approximate the data. Computing variance $\hat{\sigma}^2 = 4994.31$ of the original time series and variance $\hat{\sigma}_r^2 = 325.63$ of the residuals we can see that 93.5% $\left(\frac{\hat{\sigma}^2 - \hat{\sigma}_r^2}{\hat{\sigma}^2}.100\%\right)$ of data is explained by the trend function. In the right part of Fig. 4 we plot the autocorrelation function to see that it fulfils the above stated criterion.

For the second time series we got a logistic statistical model as the best choice with the trend function from the class $y_t = \alpha\left(1 + \beta e^{-\gamma t}\right)$ and with the best fit equal to

$$y_t = 9347.17\left(1 + 1.25797e^{-0.0837514t}\right). \tag{23}$$

The graphs od data, trend and autocorrelation function are depicted in Fig. 5. Here, the autocorrelation function is at one point slightly outside the required interval which, however, does not deteriorate the result and is caused by a numerical error. Computing again the variance $\hat{\sigma}^2 = 2.18 \times 10^6$ of the original time series and variance $\hat{\sigma}_r^2 = 20788$ of the residuals we can see that 99% of data is explained by the trend function. The shape of the trend function approaching plateau expresses the fact that the minimal volume of cells was achieved uniformly in the scanned volume (and consequently they cannot divide further) at that period of embryogenesis.

Acknowledgement

This work was supported by the European projects Embryomics and BioEmergencies and by the grants VEGA 1/3321/06 and APVV-RPEU-0004-06. We thank all the members of the Embryomics and BioEmergences projects for our very fruitful interdisciplinary interaction.

References

[1] CORSARO, S.—MIKULA, K.—SARTI, A.—SGALLARI, F.: Semi-Implicit Co-Volume Method in 3D Image Segmentation, SIAM J. Sci. Comput. **28** No. 6 (2006), 2248–2265.

[2] FROLKOVIČ, P.—MIKULA, K.: Flux-Based Level Set Method: A Finite Volume Method for Evolving Interfaces, Applied Numerical Mathematics **57** No. 4 (2007), 436–454.

[3] FROLKOVIČ, P.—MIKULA, K.—PEYRIÉRAS, N.—SARTI, A.: A Counting Number of Cells and Cell Segmentation using Advection-Diffusion Equations, Kybernetika, 2007.

[4] HANDLOVIČOVÁ, A.—MIKULA, K.—SGALLARI, F. Semi-Implicit Complementary Volume Scheme for Solving Level Set Like Equations in Image Processing and Curve Evolution: Numer. Math. **93** (2003), 675–695.

[5] KRIVÁ, Z.—MIKULA, K.—PEYRIÉRAS, N.—RIZZI, B.—SARTI, A.: Zebrafish Early Embryogenesis 3D Image Filtering by Nonlinear Partial Differential Equations, submitted.

[6] MELANI, C.—LOMBARDOT, B.—CAMPANA, M.—RIZZI, B.—ZANELLA, C.—BOURGINE, P.—MIKULA, K.—PEYRIERAS, N.—SARTI, A.: Cells Tracking in a Live Zebrafish Embryo, to appear in EMBS 2007 Proceedings.

[7] MIKULA, K.—SARTI, A.—SGALLARI, F.: Semi-Implicit Co-Volume Level Set Method in Medical Image Segmentation, in Handbook of Biomedical Image Analysis: Segmentation and Registration Models (J.Suri et al., eds.), Springer, New York, 2005, pp. 583–626.

[8] OSHER, S.—SETHIAN, J.: Fronts Propagating with Curvature Dependent Speed: Algorithm Based on Hamilton-Jacobi Formulation, J. Comput. Phys. **79** (1988), 12–49.

[9] SARTI, A.—MALLADI, R.—SETHIAN, J. A.: Proceedings of the National Academy of Sciences of the United States of America **12** No. 97 (2000), 6258–6263.

[10] ZANELLA, C.—RIZZI, B.—MELANI, C.—CAMPANA, M.—BOURGINE, P.—MIKULA, K.—PEYRIERAS, N.—SARTI, A.: Segmentation of Cells from 3D Confocal Images of Live Zebrafish Embryo, to appear in EMBS 2007 Proceedings.

Received 28 June 2007

Olga Drblíková (Mgr.), who presented talk at ISCAM 2007 conference, works as a researcher at the Department of Mathematics and Descriptive Geometry, Faculty of Civil Engineering of the Slovak University of Technology, Bratislava. She deals with computational methods based on nonlinear diffusion in image processing. Her PhD. supervisor is Doc. RNDr. Karol Mikula, DrSc.